


 Cite this: *RSC Adv.*, 2020, **10**, 24691

Electrochromic Os-based metallo-supramolecular polymers: electronic state tracking by *in situ* XAFS, IR, and impedance spectroscopies†

 Takefumi Yoshida, ^a Manas Kumar Bera, ^a Yemineni S. L. V. Narayana, ^a Sanjoy Mondal, ^a Hitoshi Abe ^{*bcd} and Masayoshi Higuchi ^{*a}

In this study, the electronic states of Os-based metallo-supramolecular polymers (**poly(OsL)²⁺**) during electrochromism were tracked by *in situ* X-ray absorption fine structure (XAFS), infrared (IR), and impedance spectroscopies. The XAFS spectra suggested electronic charge migration in the polymer, and the *in situ* spectra revealed reversible changes caused by electrochemical redox reactions. The IR spectra of the polymers showed an IVCT band, and we also confirmed the reversible changes by applying a voltage to the redox cell. During the impedance measurements, we found a drastic decrease in the charge transfer resistance (R_{CT}) of the polymer films near the electrochemical redox potential.

 Received 10th April 2020
 Accepted 9th June 2020

 DOI: 10.1039/d0ra03236k
rsc.li/rsc-advances

Introduction

Redox-active metal complexes are one of the important targets in the fields of materials science because they have various functions including conduction,¹ catalysis,² molecular magnetism,³ and electrochromism.⁴ Electrochromism is a phenomenon in which materials change their color as a result of electrochemical redox reactions. In order to understand the mechanism of electrochromism, it is important to track the oxidation state of the material. Cyclic voltammetry (CV), electron spin resonance (ESR), and X-ray absorption fine structure (XAFS) analysis are representative methods used to observe the electronic state of materials. Among the XAFS analysis methods, X-ray absorption near-edge structure (XANES) spectroscopy is useful to determine the oxidation and chemical states of metals⁵ and extended X-ray absorption fine structure (EXAFS) spectroscopy is useful to investigate the local structure around the ion.⁶ Liu and Wang have reported the electronic states of Co-based nanosheets.^{6a} Moreover, Lin has reported the XANES and EXAFS spectra of catalytic metal-organic layers to reveal the electronic states and local structures of metal ions.^{6b} Recently, *in situ* XAFS measurements have been conducted to investigate

the catalytic reactions of metal oxides.⁷ In addition, impedance spectroscopy is important to determine the charge transfer resistance of materials for their applications such as in batteries or capacitors.⁸ Kawasoko has reported a low charge transfer resistance at the Li_3PO_4 electrolyte/ $\text{Li}(\text{Ni}_{0.5}\text{Mn}_{1.5})\text{O}_4$ electrode interface and revealed that the inserted MgO layer was the origin of the impedance response.^{8a} Recently, Siroma and Itou have suggested a transmission-line model (TLM) for porous systems.^{8b,8c}

Metallo-supramolecular polymers (MSPs)⁹ are prepared by the complexation of metal ions with multitopic organic ligands. These polymers have a coordination structure composed of alternating metal ions and ligands. Previously, we have reported the electrochromic (EC) properties of MSPs.⁴ The MSPs have received significant attention for application in non-volatile displays, such as electronic papers and smart windows, because they retain their changed color without the application of any voltage. Among transition metal ions, Fe^{2+} and Ru^{2+} ions are suitable for application as metal species in polymers because of their stable redox properties, which trigger electrochromism in polymers.⁴ Recently, we have also reported Os-based metallo-supramolecular polymers (**poly(OsL)²⁺**) and their EC properties.¹⁰ These EC properties originate by the redox reaction of metal ions; however, to date, we have confirmed this only by CV (the redox potential ($E_{1/2}$): 0.94 V vs. Ag/Ag^+). Herein, we selected **poly(OsL)²⁺** among the reported MSPs and tracked their electronic states during electrochromism by *in situ* XAFS, IR, and impedance spectroscopies. XAFS spectroscopy at the Os L_3 -edge was carried out at the BL-9A and BL-12C beamline of the Photon Factory, High Energy Accelerator Research Organization (KEK).

^aElectronic Functional Macromolecules Group, National Institute for Materials Science (NIMS), Tsukuba 305-0044, Japan. E-mail: HIGUCHI.Masayoshi@nims.go.jp

^bInstitute of Materials Structure Science High Energy Accelerator Research Organization (KEK), 1-1 Oho, Tsukuba, Ibaraki 305-0801, Japan

^cDepartment of Materials Structure Science, School of High Energy Accelerator Science, SOKENDAI (The Graduate University for Advanced Studies), 1-1 Oho, Tsukuba, Ibaraki 305-0801, Japan

^dGraduate School of Science and Technology, Ibaraki University, 2-1-1 Bunkyo, Mito, Ibaraki 310-8512, Japan

† Electronic supplementary information (ESI) available. See DOI: 10.1039/d0ra03236k



Results and discussion

Tracking of EC changes by *in situ* XAFS spectroscopy

Herein, **poly(OsL)²⁺** (Fig. 1a) was synthesized by the 1 : 1 complexation of an osmium salt, $(\text{NH}_4)_2\text{OsCl}_6$, with bis(terpyridyl)benzene (**L**) according to our previous study.¹⁰ As $(\text{NH}_4)_2\text{OsCl}_6$ was used in the polymerization, it is considered that the original oxidation state of the metal complex is divalent and the counter anions in the obtained polymer are 2ClO_4^- ions. **Poly(OsL)²⁺** was obtained by the treatment of $(\text{NH}_4)_2\text{OsCl}_6$ with the counter anion ClO_4^- , as described later. In the UV-vis spectrum of methanol solution, the singlet and triplet metal-to-ligand charge transfer absorptions appeared at 511.2 and 677 nm, respectively. The color of **Poly(OsL)²⁺** is pale pink. The polymer displayed EC changes, and the color of the oxidized

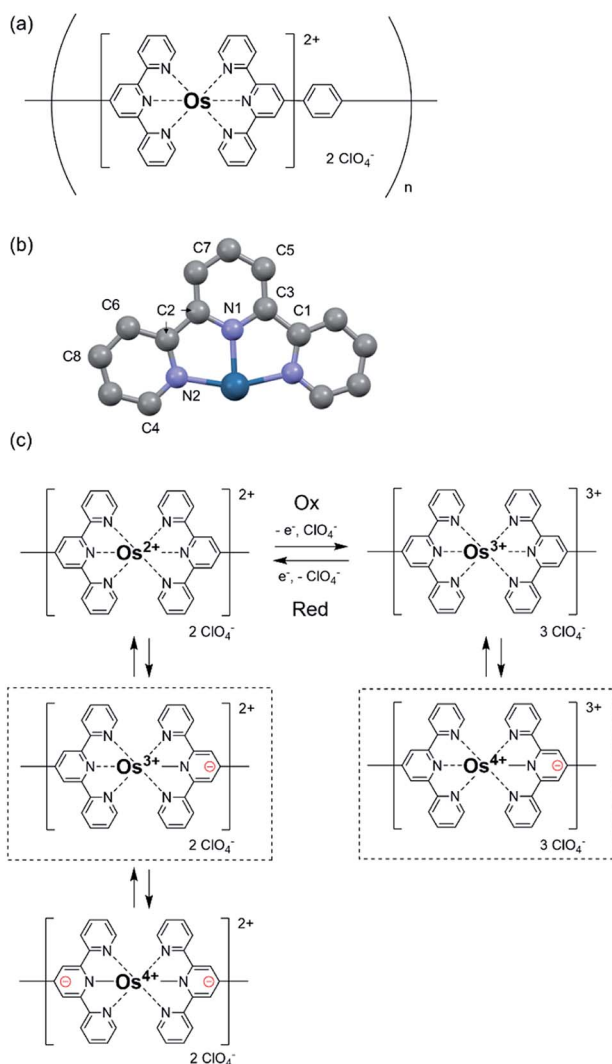


Fig. 1 (a) The molecular structure of **Poly(OsL)²⁺**. (b) The crystal structure of half of the Os complex. (c) The expected schematic for electronic charge migration in **Poly(OsL)²⁺** and **Poly(OsL)³⁺**. The complexes **Poly(OsL)²⁺** and **Poly(OsL)³⁺** highlighted with a dot frame have the major oxidation states of Os ions, as suggested by *in situ* XAFS spectroscopy.

Table 1 Coordination bond lengths around the Os ion in **Poly(OsL)²⁺**

R-Factor: 1.0%	N	R/Å	R _{eff}	Δ
N1	2	2.020	1.972	0.0485
N2	4	2.059	1.999	-0.0603
C1	1	2.872	2.868	0.0042
C2	6	2.926	2.901	0.0244
C3	1	2.841	2.934	-0.0928
C4	4	3.032	3.059	-0.0269
C5	4	4.350	4.205	0.1445
C6	4	4.287	4.248	-0.0385
C7	2	4.852	4.733	0.1190
C8	4	5.043	4.822	0.2209

polymer **Poly(OsL)³⁺** is yellow green.¹⁰ As the ClO_4^- anions compensate the change in the charges during redox reactions, **Poly(OsL)³⁺** includes three ClO_4^- anions.

Before performing *in situ* XAFS spectroscopy, we obtained the XAFS spectra of the standard samples by the transmittance method to confirm the position of the white line of both Os^{3+} and Os^{4+} ions (10 873.3 eV and 10 874.3 eV, respectively). In addition, in the EXAFS region, the fitting of the crystal structure of the reported Os complex (Fig. 1b) revealed that the Os–N coordination bond lengths in **Poly(OsL)²⁺** are 2.020 and 2.059 Å (R-factor; 1.0%, Table 1, EXAFS) (EXAFS oscillation and the Fourier transform spectra of EXAFS are shown in Fig. S1, ESI†). These values are similar to the Os–N distances determined in the crystal structure. These results suggested that the Os ion of **Poly(OsL)²⁺** has an octahedral coordination structure.¹¹ Next, for conducting *in situ* XAFS spectroscopy, we constructed a redox cell, as shown in Fig. 2a and c, with a **Poly(OsL)²⁺** film (working area: $2 \times 2.5 \text{ cm}$) on an ITO glass ($8 \Omega \text{sq}^{-1}$, $2.5 \times 2.5 \text{ cm}$). The polymer film was

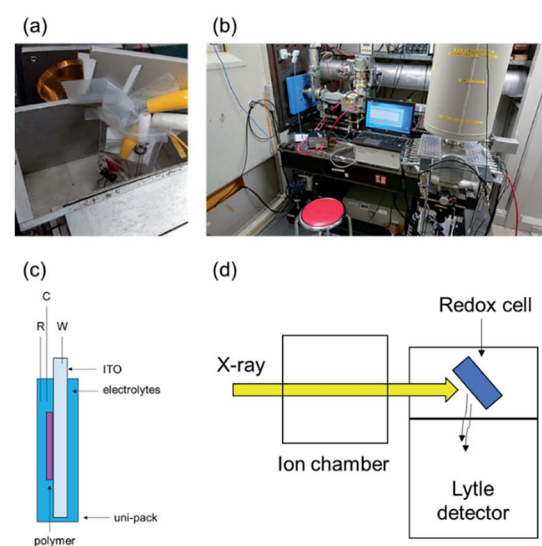


Fig. 2 (a) An image of the redox cell. (b) An image of the set up used for *in situ* XAFS spectroscopy. (c) The redox cell structure (polymer: a **Poly(OsL)²⁺** film, W: working electrode (ITO), C: counter electrode (Pt wire), R: reference electrode (Ag/Ag^+)), and electrolyte: a 0.1 M acetonitrile solution of (LiClO_4) . (d) A schematic of the measurement.



prepared by spray coating a methanol solution of **poly(OsL)²⁺** (5 mg ml⁻¹, mass concentration of the Os ion was ~20%) on the ITO glass. The polymer film was washed with a 0.1 M acetonitrile solution of LiClO₄ to change the counter anion from Cl⁻ to ClO₄⁻, as shown in Fig. 1a. We used the polymer-coated ITO glass as a working electrode, the 0.1 M acetonitrile solution of LiClO₄ as an electrolyte solution, a Pt wire as a counter electrode, and Ag/Ag⁺ as a reference electrode. We replaced the quartz cuvette with Uni-Pak (zipper bag) and maintained the distance between the **poly(OsL)²⁺** film and Uni-Pak or the thickness of the electrolyte at less than 1 mm to decrease the absorption of both the cell and the electrolyte. Then, we measured the XAFS spectra of the original-state **poly(OsL)²⁺** and the oxidized-state **poly(OsL)³⁺** in the fluorescence yield mode using a Lytle detector by applying a potential of 0 V and 0.9 V vs. Ag/Ag⁺ (ref. 10) to the redox cell (Fig. 2b and d), respectively.

The *in situ* XAFS spectra of **poly(OsL)²⁺** are shown in Fig. 3a. The position of the white line in the XANES region represents the oxidation state of the metal atom. The white line of OsCl₃ is at 10 873.3 eV and that of a **poly(OsL)²⁺** pellet is at 10 873.9 eV. Interestingly, these results suggest that the oxidation state of

Table 2 The ratios of Os³⁺ (10 873.3 eV) to Os⁴⁺ (10 874.3 eV) calculated by curve fitting the XAFS spectra of **poly(OsL)²⁺**, **poly(OsL)³⁺**, and electrochemically reduced **poly(OsL)³⁺**

	Poly(OsL) ²⁺	Poly(OsL) ³⁺	Reduced poly(OsL) ³⁺
Os ³⁺	0.64	0.16	0.60
Os ⁴⁺	0.36	0.84	0.40

the osmium ion in **poly(OsL)²⁺** is Os³⁺ or higher.¹² However, a divalent state is strongly suggested in many complexes synthesized using Os²⁺ salts.¹³ Therefore, we speculate that the direct detection of an Os³⁺ species in the XAFS spectrum was caused by electronic charge migration, such as the formation of Os³⁺·[terpyridine]⁻, inside the metal complex moieties of **poly(OsL)²⁺** (Fig. 1c).

Furthermore, when the polymer was oxidized to **poly(OsL)³⁺** by applying an oxidation potential (0.9 V vs. Ag/Ag⁺), the white line moved to a further higher-energy region (10 874.2 eV). It has been reported that the energy difference between Os³⁺ and Os⁴⁺ is about 1 eV.¹⁴ As the white line of Os³⁺ appeared at 10 873.3 eV in the spectrum, the observed value of 10 874.3 eV represents the white line of Os⁴⁺. According to our consideration that the Os³⁺ species is observed in **poly(OsL)²⁺**, the observation of Os⁴⁺ suggests the formation of **poly(OsL)³⁺**. In contrast, when a reduction potential (0.0 V vs. Ag/Ag⁺) was applied to the **poly(OsL)³⁺** film, the white line returned to 10 873.5 eV. This indicates that the Os⁴⁺ ions of **poly(OsL)³⁺** were again electrochemically reduced to Os³⁺. We changed the applied potentials (0.0 and 0.9 V vs. Ag/Ag⁺) for five times and confirmed the repeatability of the spectral changes.

The electronic states of **poly(OsL)²⁺**, **poly(OsL)³⁺**, and electrochemically reduced **poly(OsL)³⁺** were further analyzed by curve fitting the spectra with the two peaks of 10 873.3 eV (Os³⁺) and 10 874.3 eV (Os⁴⁺). The fitting profile of **poly(OsL)²⁺** is shown in Fig. 3b. The results of peak separation are summarized in Table 2, which reveal that both Os³⁺ and Os⁴⁺ exist in the polymers. However, the ratio of Os³⁺ to Os⁴⁺ was different among the polymers. In **poly(OsL)²⁺**, the proportion of Os³⁺ is major (64%). On the other hand, Os⁴⁺ is prominent in **poly(OsL)³⁺**. In electrochemically reduced **poly(OsL)³⁺**, the ratio of Os³⁺ to Os⁴⁺ was similar to that in **poly(OsL)²⁺**. These results support that **poly(OsL)³⁺** is electrochemically reduced to original **poly(OsL)²⁺**.

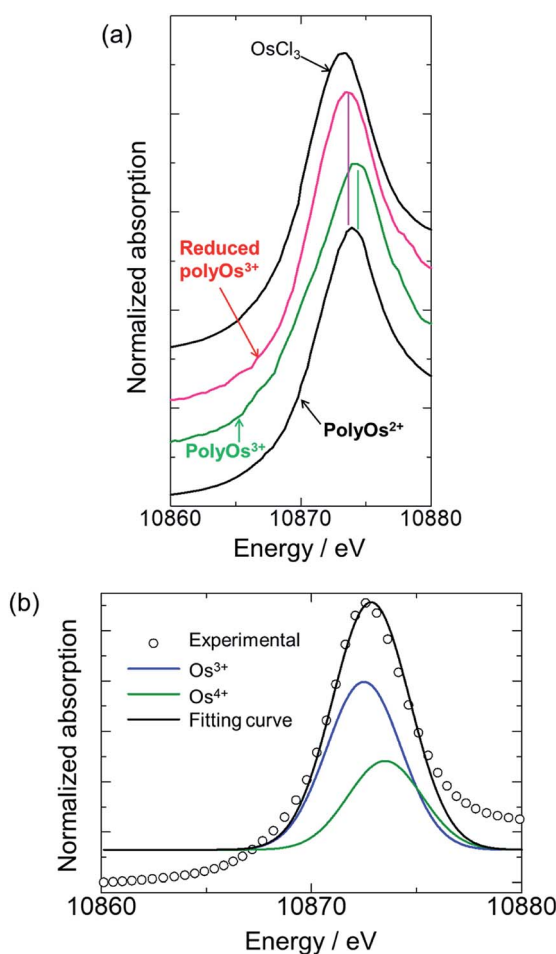


Fig. 3 XAFS spectra at the Os L₃-edge (a) XANES spectra: black: references (OsCl₃ and **poly(OsL)²⁺**), green: **poly(OsL)³⁺** at 0.9 V, and pink: reduced **poly(OsL)³⁺** at 0.0 V. (b) The XANES data analysis of **poly(OsL)²⁺** by a curve fitting method.

Tracking of EC changes by IR measurements

The electronic charge migration shown in Fig. 1c was also supported by the IR spectrum of **poly(OsL)²⁺** (Fig. S2 and ESI†). The large absorption band at ~3300 cm⁻¹ (~0.41 eV) in the spectrum of **poly(OsL)²⁺** (Fig. 4a) can be attributed to the intervalence charge transfer (IVCT) between Os³⁺ and Os⁴⁺ in **poly(OsL)²⁺** (in the spectrum, the band at 3180 cm⁻¹ is assigned to the used KCl pellet). The fine modulation at 3600–3900 cm⁻¹ is due to water vapors in the air. We used the spectrum of ITO as the background spectrum; however, there is a small influence of ITO because of scattering. In order to exclude “arbitrariness”,

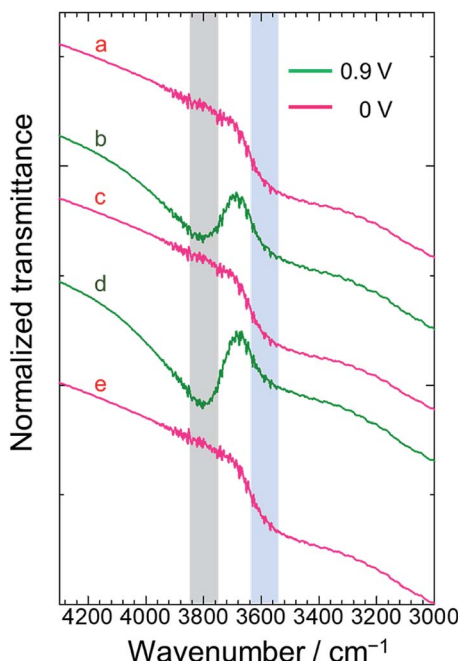


Fig. 4 IR spectra of (a) poly(OsL)^{2+} and (b–e) the polymer film repeatedly oxidized/reduced at 0.9 V or 0 V vs. Ag/Ag^+ , respectively. ((b) The first oxidation to poly(OsL)^{3+} ; (c) the reduction of (b); (d) the second oxidation of (c); and (e) the reduction of (d)).

the spectrum was not treated by any baseline corrections or smoothing.

In order to obtain further evidence of IVCT, we measured the IR spectrum of poly(OsL)^{3+} prepared by the electrochemical oxidation of poly(OsL)^{2+} as follows. The poly(OsL)^{2+} film on the ITO glass was oxidized to poly(OsL)^{3+} by applying an oxidation potential (0.9 V vs. Ag/Ag^+) to the redox cell until the film changed from pale pink to yellow green. Then, the polymer film was taken out from the cell and washed with acetonitrile. The yellow green color of the polymer film confirms that the oxidation state was retained even after the washing step. The IR spectrum of the obtained poly(OsL)^{3+} film in the range of 3000–4300 cm^{-1} is shown in Fig. 4b. Interestingly, a new peak appeared around 3800 cm^{-1} ($\sim 0.47 \text{ eV}$) in the spectrum. The slightly higher energy band than the IVCT band of poly(OsL)^{2+} could be assigned to the inter-polymer IVCT through the counter anion (ClO_4^-) because poly(OsL)^{3+} has 1.5 times more counter anions than poly(OsL)^{2+} to maintain the charge balance. Then, the poly(OsL)^{3+} film was again reduced at 0.0 V vs. Ag/Ag^+ . The spectrum of poly(OsL)^{3+} after reduction (Fig. 4c) was quite similar to that of original poly(OsL)^{2+} . By varying the oxidation state of the polymer film for four times (Fig. 4b–e), we confirmed the repeatability of the IR spectral changes. Although electrochemical IR measurement itself is a general method,¹⁵ this is the first report where IR spectral changes were observed during electrochromism in MSPs.

Tracking of EC changes by impedance spectroscopy

For the further investigation of the EC properties of poly(OsL)^{2+} , we tracked the impedance response. At first, we measured the

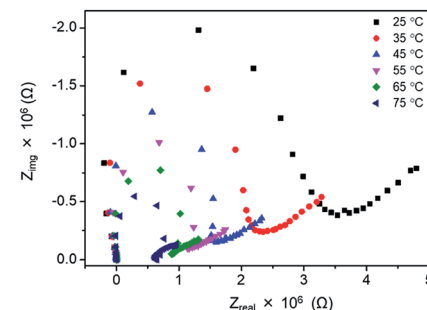


Fig. 5 Nyquist plots of poly(OsL)^{2+} at various temperatures and 50% RH.

impedance spectra of a poly(OsL)^{2+} pellet using a two-probe method without applying any DC voltage. The impedance response at various temperatures is shown in Fig. 5. The ion conductivities of the polymer pellet at 25, 35, 45, 55, 65, and 75 °C and 50% RH (same as the ambient atmosphere) were calculated to be 3.00×10^{-7} , 4.38×10^{-7} , 5.80×10^{-7} , 7.28×10^{-7} , 8.72×10^{-7} , and $1.28 \times 10^{-6} \text{ S cm}^{-1}$, respectively, by the x-axis intercept of the semicircle at higher frequencies (Table S1 and ESI†). The activation energy for the ion conductivity was

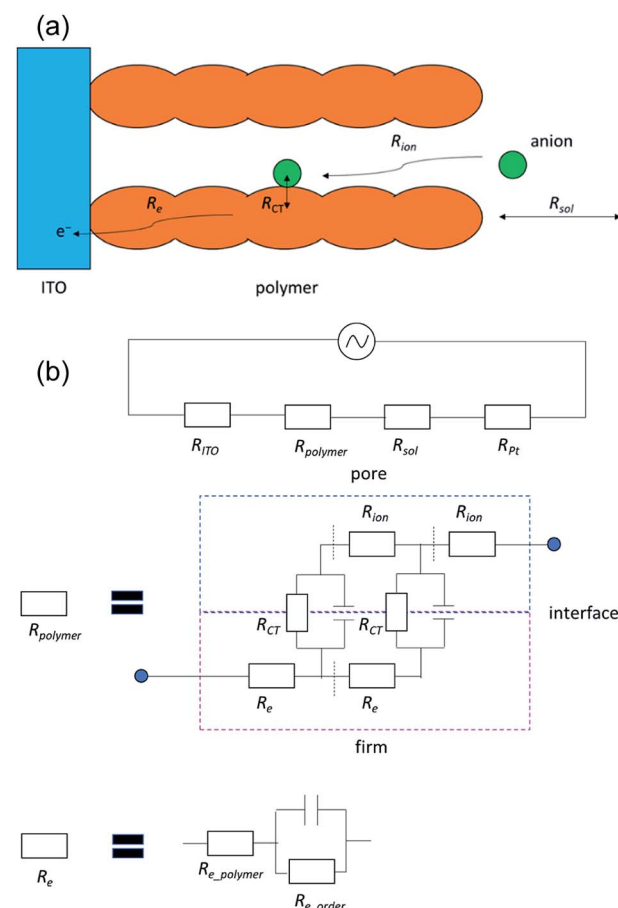


Fig. 6 (a) The transmission-line model. (b) Circuits for the transmission-line model.



calculated to be 0.24 eV by Arrhenius plots (Fig. S3 and ESI†). This value was significantly smaller than that of an Fe-based MSP, **poly(FeL)²⁺** (*cf.* 2.5 eV).¹⁶

Next, we investigated the effect of deuterium on the ion conductivity. We immersed a pellet of **poly(OsL)²⁺** in both H₂O (control) and D₂O (replacing H₂O with D₂O) for 30 min to prepare **poly(OsL)^{2+H}** and **poly(OsL)^{2+D}**. Then, the ion conductivity was measured at RT (Fig. S4 and S5, ESI†). The ion conductivities of **poly(OsL)^{2+H}** and **poly(OsL)^{2+D}** were calculated to be 2.07×10^{-5} and 3.67×10^{-6} S cm⁻¹, respectively, by the Nyquist plots. These results indicate that the hydrogen atoms of water molecules act as ion carriers.

Next, we investigated the impedance changes of the polymer pellet by applying 1.0 V; however, we observed only a noisy signal because of the low electronic conductivity of the polymer. Therefore, we prepared a **poly(OsL)²⁺** film on an ITO glass and measured its impedance response using the three-probe method at liquid–solid interfaces (open-Q) and various potentials (0.0–1.2 V *vs.* Ag/Ag⁺) with a 10 mV AC amplitude (the same setup as the redox cell used for XAFS spectroscopy). Herein, we used a transmission-line model (Fig. 6 and 7a).⁸ The impedance responses of **poly(OsL)²⁺** at liquid–solid interfaces are shown in Fig. 7b and S6, ESI.† The ionic resistivity (R_{ion}) and resistivity of the electrolyte (R_{sol}) were calculated to be 68.8 and 80.5 Ω cm², respectively. These values are constant in this system. In the range of 0.0–0.6 V *vs.* Ag/Ag⁺ at a 10 mV AC amplitude, the slope of the Nyquist plots gradually declines and shows a semicircle because of the decrease in the charge-transfer resistance (R_{CT}). On the other hand, in the range of 0.6–1.2 V *vs.* Ag/Ag⁺ at a 10 mV AC amplitude, the slope of the Nyquist plots gradually increases because of the increase in R_{CT} . At 0.6 V, there are two semicircles of electron resistivity (R_{e}) and R_{CT} . The R_{e} is composed of the resistivity of the polymer itself ($R_{\text{e,polymer}}$), the resistivity raised from the ordering of polymer chains ($R_{\text{e,order}}$) (if there are many junctions among the polymer chains, it will increase). Herein, it is

almost dominant in R_{e}), and the resistivity of the capacitor. The $R_{\text{e,order}}$ was calculated to be 28 Ω cm². The values of R_{CT} at 0.3–0.8 V *vs.* Ag/Ag⁺ were calculated to be 547, 149, 196, 137, 196, and 839 Ω cm² using the semicircle (Fig. 7c). These values are as high as the values (\sim 200–2000 Ω cm²) reported for the electrode/solid electrolyte interface.¹⁷ To investigate the relationship with the EC change, we measured the UV-vis spectra of the polymer film at various potentials (Fig. 7d). There is no difference between the transmittance at 500 nm in the ranges of 0.0–0.5 V and 0.7–0.9 V *vs.* Ag/Ag⁺, whereas large spectral changes occurred in the range of 0.5–0.7 V *vs.* Ag/Ag⁺. These large changes in the abovementioned range are consistent with the charge transfer process occurring during electrochromism. Remarkably, there is no difference between the transmittance at 500 nm; however, we observed a charge transfer process especially at 0.3 V, 0.4 V, and 0.8 V. These phenomena indicate that **poly(OsL)²⁺** and **poly(OsL)³⁺** already have different oxidation states of osmium ions (Os³⁺ and Os⁴⁺) in them due to electron migration, which is shown in Fig. 1c.

Conclusions

In summary, we established a method to track the electronic states of MSPs during electrochromism by *in situ* XAFS, IR, and impedance spectroscopies. The XAFS spectra suggested electronic charge migration in the Os-based metallocsupramolecular polymers (**poly(OsL)²⁺**) and the reversible changes caused by the electrochemical redox reactions. The IR spectra showed the IVCT band attributed to the electronic charge migration in the polymer, and the reversible changes were confirmed by applying a voltage to the redox cell. The impedance spectra revealed a drastic decrease in the charge transfer resistance (R_{CT}) of the polymer film around the electrochemical redox potential. These techniques are widely applicable to other redox-active MSPs and metal complexes.

Experimental

Preparation of **poly(OsL)²⁺**

Poly(OsL)²⁺ was synthesized by the same procedure as reported in the literature.¹⁰ The polymer film (working area 2 cm × 2.5 cm) on ITO (8 Ω sq⁻¹, 2.5 cm × 2.5 cm) was prepared by a spray coating method using 5 mg ml⁻¹ of a methanol solution of **Poly(OsL)²⁺**.

XAFS spectroscopy

XAFS spectroscopy was carried out at the BL-9A (energy: 2.1–15 keV, energy resolution: $\Delta E/E \sim 2 \times 10^{-4}$ (9 keV), photon flux at sample position: 6×10^{11} phs per s (7 keV), monochromator: Si(111) water-cooled double crystal, focusing mirror: double bent conical mirror (Rh coated), beam size (FWHM): 0.5 mm × 0.3 mm), BL-12C (energy: 4–23 keV, energy resolution: $\Delta E/E \sim 2 \times 10^{-4}$, photon flux at sample position: 9×10^{10} phs per s (8 keV), monochromator: Si(111), focusing mirror: double bent conical mirror (Rh coated), beam size (FWHM): 0.6 mm × 0.5 mm) beamline of the

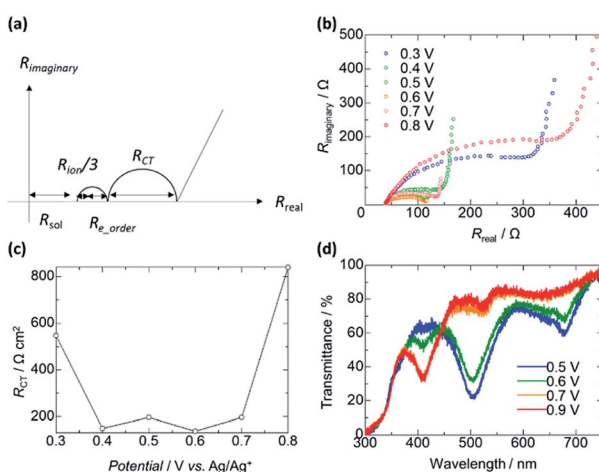


Fig. 7 (a) The model of impedance responses. (b) Impedance responses of a **poly(OsL)²⁺** film on an ITO glass at 0.3–0.8 V *vs.* Ag/Ag⁺. (c) The R_{CT} at various potentials. (d) UV-vis spectra of a **polyOs** film on an ITO glass at 0.5–0.9 V *vs.* Ag/Ag⁺.

photon factory (ring energy: 2.5 GeV, max. current: 450 mA (usually top-up operation), critical energy: 4 keV, horizontal acceptance: 3 mrad), High Energy Accelerator Research Organization (KEK) (the edge position was calibrated by that of the Os metal powder and Pt foil). Analysis was performed using the Demeter software platform. We used the reported crystal data for calculating F_{eff} .⁹

Spectroscopy

FTIR spectra were acquired using the FTIR-8400S infrared spectrophotometer. UV-vis spectra were obtained by an Ocean spectrometer (Ocean Optics, Inc.).

Electrochemistry

The Solartron 1260 Impedance gain/phase analyser coupled with the Solartron 1296 dielectric interface and Princeton Applied Research VersaSTAT 4 were used for the impedance spectroscopy. Working electrode: ITO, counter electrode: Pt wire, reference electrode: Ag/Ag⁺, and supporting electrolyte: 0.1 M MeCN solution of LiClO₄.

Conflicts of interest

There are no conflicts to declare.

Acknowledgements

This research was financially supported by the JST-CREST project (grant number: JPMJCR1533) and TIA “Kakehashi” program. The X-ray absorption fine structure was investigated at the BL-9A, 12C beamline in the Photon Factory of High Energy Accelerator Research Organization (KEK, Proposal No. 2019G117, 2017P016, No. 2017PF-04).

Notes and references

- (a) K. Wada, K. Sakaushi, S. Sasaki and H. Nishihara, *Angew. Chem., Int. Ed.*, 2018, **57**, 8886–8890; (b) L. S. Xie, L. Sun, R. Wan, S. S. Park, J. A. DeGayner, C. H. Hendon and M. Dincă, *J. Am. Chem. Soc.*, 2018, **140**, 7411–7414.
- (a) A. Li, H. Ooka, N. Bonnet, T. Hayashi, Y. Sun, Q. Jiang, C. Li, H. Han and R. Nakamura, *Angew. Chem., Int. Ed.*, 2019, **58**, 5054–5058; (b) S. Lin, P. M. Usov and A. J. Morris, *Chem. Commun.*, 2018, **54**, 6965–6974.
- J. Tong, S. Demeshko, M. John, S. Dechert and F. Meyer, *Inorg. Chem.*, 2016, **55**, 4362–4372.
- (a) M. Higuchi and D. G. Kurth, *Chem. Rec.*, 2007, **7**, 203–209; (b) F. Han, M. Higuchi and D. G. Kurth, *J. Am. Chem. Soc.*, 2008, **130**, 2073–2081; (c) B.-H. Chen, S.-Y. Kao, C.-W. Hu, M. Higuchi, K.-C. Ho and Y.-C. Liao, *ACS Appl. Mater. Interfaces*, 2015, **7**, 25069–25076; (d) M. Higuchi, *J. Mater. Chem. C*, 2014, **2**, 9331–9341; (e) C.-W. Hu, T. Sato, J. Zhang, S. Moriyama and M. Higuchi, *J. Mater. Chem. C*, 2013, **1**, 3408–3413.
- H. Abe, Y. Niwa, M. Kitano, Y. Inoue, T. Yokoyama, M. Hara and H. Hosono, *Bull. Chem. Soc. Jpn.*, 2017, **90**, 963–965.
- (a) Z. Chen, Y. Song, J. Cai, X. Zheng, D. Han, Y. Wu, Y. Zang, S. Niu, Y. Liu, J. Zhu, X. Liu and G. Wang, *Angew. Chem., Int. Ed.*, 2018, **57**, 5076–5080; (b) Z. Lin, N. C. Thacker, T. Sawano, T. Drake, P. Ji, G. Lan, L. Cao, S. Liu, C. Wang and W. Lin, *Chem. Sci.*, 2018, **9**, 143–151; (c) A. Garai, S. Sobottka, R. Schepper, W. Sinha, M. Bauer, B. Sarkar and S. Kar, *Chem.-Eur. J.*, 2018, **24**, 12613–12622; (d) H. Ohtsu, T. D. Bennett, T. Kojima, D. A. Keen, Y. Niwa and M. Kawano, *Chem. Commun.*, 2017, **53**, 7060–7063.
- (a) M. W. Kanan, J. Yano, Y. Surendranath, M. Dincă, V. K. Yachandra and D. G. Nocera, *J. Am. Chem. Soc.*, 2010, **132**, 13692–13701; (b) S. R. Bare, S. D. Kelly, B. Ravel, N. Greenlay, L. King and G. E. Mickelson, *Phys. Chem. Chem. Phys.*, 2010, **12**, 7702–7711.
- (a) H. Kawasoko, S. Shiraki, T. Suzuki, R. Shimizu and T. Hitosugi, *ACS Appl. Mater. Interfaces*, 2018, **10**, 27498–27502; (b) Z. Siroma, N. Fujiwara, S. Yamazaki, M. Asahi, T. Nagai and T. Ioroi, *Electrochim. Acta*, 2015, **160**, 313–322; (c) N. Ogihara and Y. Itou, *R&D Rev. Toyota CRDL*, 2017, **48**, 17–24; (d) N. U. Day, M. G. Walter and C. C. Wamser, *J. Phys. Chem. C*, 2015, **119**, 17378–17388; (e) N. Ogihara, S. Kawauchi, C. Okuda, Y. Itou, Y. Takeuchi and Y. Ukyo, *J. Electrochem. Soc.*, 2012, **159**, A1034–A1039.
- (a) J. B. Beck and S. J. Rowan, *J. Am. Chem. Soc.*, 2003, **125**, 13922–13923; (b) A. Winter and U. S. Schubert, *Chem. Soc. Rev.*, 2016, **45**, 5311–5357.
- M. K. Bera, C. Chakraborty, U. Rana and M. Higuchi, *Macromol. Rapid Commun.*, 2018, **39**(1–6), 1800415.
- D. C. Craig, M. L. Scudder, W.-A. McHale and H. A. Goodwin, *Aust. J. Chem.*, 1998, **51**, 1131.
- Y. Takahashi, T. Uruga, K. Suzuki, H. Tanida, Y. Terada and K. H. Hattori, *Geochim. Cosmochim. Acta*, 2007, **71**, 5180–5190.
- (a) B. Happ, A. Winter, M. D. Hager and U. S. Schubert, *Chem. Soc. Rev.*, 2012, **41**, 2222–2255; (b) M.-J. Sun, J.-Y. Shao, C.-J. Yao, Y.-W. Jhong and J. Yao, *Inorg. Chem.*, 2015, **54**, 8136–8147; (c) F. Barigelli, L. Flamigni, M. Guardigli, A. Juris, M. Beley, S. Chodorowski-Kimmes, J.-P. Collin and J.-P. Sauvage, *Inorg. Chem.*, 1996, **35**, 136–142; (d) J.-Y. Shao and Y.-W. Zhong, *Inorg. Chem.*, 2013, **52**, 6464–6472; (e) M. Lahav and M. E. van der Boom, *Adv. Mater.*, 2018, 1706641.
- Y. Yamashita, Y. Takahashi, H. Haba, S. Enomoto and H. Shimizu, *Geochim. Cosmochim. Acta*, 2007, **71**, 3458–3475.
- (a) H. Wang, Y.-W. Zhou and W.-B. Cai, *Curr. Opin. Electrochem.*, 2017, **1**, 73–79; (b) Y. Tanaka, M. Ono and M. Akita, *J. Porphyrins Phthalocyanines*, 2015, **19**, 442–450.
- R. K. Pandey, M. D. Hossain, T. Sato, U. Rana, S. Moriyama and M. Higuchi, *RSC Adv.*, 2015, **5**, 49224–49230.
- (a) C. Yada, A. Ohmori, K. Ide, H. Yamasaki, T. Kato, T. Saito, F. Sagane and Y. Iriyama, *Adv. Energy Mater.*, 2014, **4**, 1301416; (b) J. Li, C. Ma, M. Chi, C. Liang and N. Dudney, *Adv. Energy Mater.*, 2015, **5**, 1401408.

